RevMexAA (Serie de Conferencias), **36**, CD266–CD271 (2009)

POLARIZED EMISSION OF EDGE-ON GALAXIES IN COMPARISSON WITH THE COSMIC-RAY DRIVEN DYNAMO MODEL

K. Otmianowska-Mazur,[1] M. Hanasz,[2] M. Soida,[1] B. Kulesza-Żydzik,[1] and G. Kowal[1,3]

RESUMEN

Construímos mapas de emisión sincrotrón polarizada en radio de una galaxia entera, basados en modelos locales del dínamo forzado por rayos cósmicos. Realizamos simulaciones numéricas del dínamo en dominios Cartesianos, con condiciones a la frontera cortantes-periódicas, localizadas a diferentes radios galactocéntricos. Las soluciones locales son acumuladas para construir imágenes de sincrotrón de la galaxia completa. El principal objetivo de este trabajo es el de comparar resultados de modelos con observaciones en el radio contínuo de galaxias espirales casi de canto.

En base a la estructura magnética modelada se construyeron mapas de polarización con diferentes ángulos respecto al plano del cielo. Finalmente los mapas son convueltos con un patrón de telescopio dado. Mostramos que es posible reconstruir las estructuras extendidas en el halo de galaxias de canto (las llamadas estructuras con forma de X). Más aún, demostramos que los valores de los ángulos de apertura de los vectores de polarización en mapas de cara son similares a los observados en galaxias reales.

ABSTRACT

We construct maps of polarized synchrotron radio emission of a whole galaxy, based on local models of the cosmic ray (CR) driven dynamo. We perform numerical simulations of the dynamo in local Cartesian domains, with shear-periodic boundary conditions, placed at different galactocentric radii. Those local solutions are concatenated together to construct the synchrotron images of the whole galaxy. The main aim of the paper is to compare the model results with the observed radio continuum emission from nearly edge-on spiral galaxy.

On the basis of the modeled magnetic structure the polarization maps at different viewing angles are prepared, using the distribution of cosmic-ray electrons obtained from numerical simulations. Finally, our maps are convolved with the given radiotelescope beam. We show that it is possible to reconstruct the extended magnetic halo structures of the edge-on galaxies (so called X-shaped structures). Moreover, we demonstrate that the values of the pitch angles of polarization vectors on the face-on maps are similar to the ones observed in real galaxies.

Key Words: cosmic rays — galaxies: magnetic fields — techniques: numerical simulations

1. GENERAL

New radio-continuum observations of the polarized emission made at centimeter wavelengths of edge-on spiral galaxies (Tüllmann et al. 2000; Soida 2005; Heesen et al. 2005) showed a characteristic magnetic field structure. Nowadays, the observed magnetic polarization vector directions in the halo are oriented at a large angle to the galactic disk, while earlier observations limited by sensitivity demonstrated mainly plane-parallel magnetic field component (e.g. Dumke et al. 1995). As an example of such structure the polarization map of the galaxy NGC 4666, where the topolines of total power at 6 cm and polarized vectors are superimposed onto the optical map of this galaxy is presented in Figure 1 (Soida 2005). We see that in the disk the polarization vectors are generally parallel to the galactic plane, while in the halo their angles are much higher forming a kind of X-shaped configuration. Similar structures of the polarization vectors in halos are observed for other galaxies (NGC 5775, Tüllmann et al. 2000; NGC 4217, NGC 3628, NGC 4631, NGC 891, Soida 2005; NGC 253, Heesen et al. 2005). What is more Tüllmann et al. (2000) found that NGC 5775 showed the differential rotation in the direction perpendicular to the disk. This fact could be very important in obtaining the observed X-shaped structure of magnetic polarized vectors.

Still, we do not know which physical process could be responsible for formation of such extended magnetic structures in the halo. The turbulent dy-

[1]Obserwatorium Astronomiczne UJ ul. Orla 171, 30-244 Kraków, Poland.
[2]Centre for Astronomy, Nicolaus Copernicus University, Toruń, Poland.
[3]McMaster University, Hamilton, Canada.

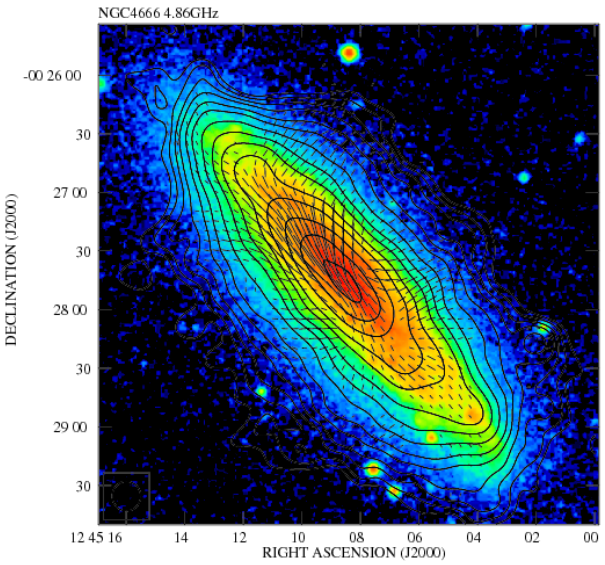

Fig. 1. The contour plot of total power emission at 4.8 GHz with polarization magnetic vectors, superimposed onto optical picture of NGC 4666.

namo theory, which apply the magnetic field amplification due to turbulent motions and shear in spiral galaxies, failed in its trials to get the galactic large-scale magnetic fields amplification (e.g. Widrow 2002; Hanasz et al. 2004; Otmianowska-Mazur et al. 2007; Brandenburg & Dobler 2001; Brandenburg & Sokoloff 2002). In opposition to that, our model of the cosmic-ray driven dynamo showed that due to a presence of a range of realistic physical processes it was possible to increase 10^5 times the total energy of the large-scale azimuthal component of galactic magnetic field in timescale of 140 Myr (Hanasz et al. 2004, 2006). The new results of modelling the whole disk of the galaxy NGC 5775 constructed from set of local volumes placed at different distances from the galactic center are presented in this paper. Our final maps give the outcome of integration of synchrotron emissivities (Stokes I, Q and U) along the line of sight, oriented according to that of real galaxy NGC 5775 and compared with polarized radio continuum observations made at 6 cm (Tüllmann et al. 2000).

2. NUMERICAL MODEL OF THE COSMIC-RAY DRIVEN DYNAMO

2.1. *Importance of cosmic rays for ISM dynamics*

The major source of ISM disturbances are SN type II explosions (Mac Low & Klessen 2004) with the kinetic energy around $\sim 10^{51}$ erg. 10% of this energy (even 50%, Ellison et al. 2004) could accelerate cosmic rays in shocks to relativistic energies. The principle of action of our model of the cosmic ray driven dynamo (Hanasz et al. 2004, 2006) is based on this cosmic ray energy, which is supplied to the disk by SN explosions. It was shown that the galactic disk including gas, magnetic field and cosmic rays, stratified by vertical gravity is unstable against the Parker instability (Parker 1992). Buoyancy effects induce vertical and horizontal motions of the fluid and formation of magnetic loops in the initial predominantly horizontal magnetic fields. The Coriolis force present due to the galactic rotation implies a coherent twisting of the loops, which leads to the grow of the small-scale radial magnetic field components. Later, these loops merge to the large-scale ones, by the magnetic reconnection process (Kowal et al. 2003; Hanasz et al. 2004, 2006). Finally, differential rotation stretches the radial magnetic field to amplify the large-scale azimuthal magnetic field, what results in an exponential growth of the large scale magnetic field. The timescale of magnetic field amplification, resulting from the action of CR-driven dynamo, has been found (Hanasz et al. 2004, 2006) to be close, in typical galactic conditions, to 140 Myr, which is two times shorter than the galactic rotation timescale.

2.2. *Cosmic ray transport*

Particle diffusion numerical experiments (e.g. Giaccalone & Jokipii 1999; Jokipii 1999) showed that the diffusion of the cosmic rays is anisotropic along the magnetic field lines. They gave also the values of the diffusion coefficients of the cosmic rays along and perpendicular to the magnetic field lines: $K_{\parallel} \sim 10^{28} - 10^{29}$ cm^2 s^{-1}, $K_{\perp}/K_{\parallel} \sim 0.05$. In order to study the dynamical role of the cosmic rays in the galactic disk we localy solve the MHD equations together with the diffusion-advection equation with the diffusion tensor of cosmic rays given by Schlickeiser & Lerche (1985):

$$\frac{\partial e_{\rm cr}}{\partial t} + \boldsymbol{\nabla}(e_{\rm cr}\boldsymbol{V}) = -p_{\rm cr}\boldsymbol{\nabla}\boldsymbol{V} + \boldsymbol{\nabla}(\hat{K}\boldsymbol{\nabla}e_{\rm cr}) + \text{CR sources (SN remnants)}\,, \quad (1)$$

$$p_{\rm cr} = (\gamma_{\rm cr} - 1)e_{\rm cr}\,, \quad (2)$$

with

$$\gamma_{\rm cr} = 14/9\,. \quad (3)$$

We apply anisotropic diffusion of CRs (e.g. Ryu et al. 2003; Hanasz & Lesch 2003) in the following way:

$$K_{ij} = K_{\perp}\delta_{ij} + (K_{\parallel} - K_{\perp})n_i n_j, \quad n_i = B_i/B, \quad (4)$$

TABLE 1

PARAMETERS AND MAIN RESULTS OF MODELS EXAMINED IN THIS PAPER

Vertical gravity at $R =$ [kpc]	5.0	5.5	6.0	6.5	7.0	7.5	8.0	8.5	9.0	9.5	10.0
Gas column density $\times 10^{20}$	27	25	22	18	16	14	11	10	9	8.5	8
Angular velocity Ω [Myr^{-1}]	0.050	0.045	0.040	0.038	0.035	0.033	0.030	0.028	0.025	0.024	0.022
SN rate [kpc^{-2} Myr^{-1}]	130	120	100	80	60	50	30	25	20	15	10
Magn. flux growth time τ [Myr]	152	165	176	182	196	206	223	253	263	286	283
Pitch angle at $t = 700$ Myr [°]	10	10	10	10	10	11	12	12	12	12	12
Wind velocity [km/s]	96	86	87	82	77	74	68	68	60	58	65

Other implementations of CRs in MHD codes were presented also by Kuwabara et al. (2004), and Snodin et al. (2006) with a more accurate description of CR diffusion and confinement.

2.3. *Dynamics of magnetized ISM with cosmic rays*

In our model we apply the following set of resistive MHD equations

$$\frac{\partial \rho}{\partial t} + \boldsymbol{\nabla} \cdot (\rho \boldsymbol{V}) = 0\,, \tag{5}$$

$$\frac{\partial e}{\partial t} + \boldsymbol{\nabla} \cdot (e \boldsymbol{V}) = -p\,(\boldsymbol{\nabla} \cdot \boldsymbol{V})\ , \tag{6}$$

$$\frac{\partial \boldsymbol{V}}{\partial t} + (\boldsymbol{V} \cdot \boldsymbol{\nabla})\boldsymbol{V} = -\frac{1}{\rho}\boldsymbol{\nabla}\left(p + p_{\rm cr} + \frac{B^2}{8\pi}\right) + \frac{\boldsymbol{B} \cdot \boldsymbol{\nabla} \boldsymbol{B}}{4\pi\rho} - 2\boldsymbol{\Omega} \times \boldsymbol{v} + 2q\Omega^2 \mathrm{x}\hat{\boldsymbol{e}}_{\rm x}\,, \tag{7}$$

$$\frac{\partial \boldsymbol{B}}{\partial t} = \boldsymbol{\nabla} \times (\boldsymbol{V} \times \boldsymbol{B}) + \eta \Delta \boldsymbol{B}\,,, \tag{8}$$

$$p = (\gamma - 1)e, \quad \gamma = 5/3\,, \tag{9}$$

where $q = -\mathrm{d}\ \ln\ \Omega/\mathrm{d}\ \ln\ \mathrm{R}$ is the shearing parameter, (R is the distance to galactic center), η is the resistivity, γ is the adiabatic index of thermal gas, the gradient of cosmic ray pressure $\nabla p_{\rm cr}$ is included in the equation of motion (see eg. Berezinski et al. 1990) and other symbols have their usual meaning. The thermal gas component is currently treated as an adiabatic medium.

We apply local Cartesian coordinates x, y, z which are parallel to the global galactic r, ϕ and z axes, respectively. We construct the polarization maps of an edge-on galaxy characterized by a high halo, so we assume that our local simulation are extended up to 4 kpc above and below the disk. The local cube dimension in the x direction is equal to 500 pc and in y to 1000 pc. The resolution of our local calculations is given by 25 × 50 × 400 grid points. The cosmic ray diffusion coefficients assumed in the simulations are: $K_{\parallel} = 3 \times 10^{27} \mathrm{cm}^2\ \mathrm{s}^{-1}$ and $K_{\perp} = 3 \times 10^{26}\ \mathrm{cm}^2\ \mathrm{s}^{-1}$. These values are smaller than expected realistic values, referenced above, due to the timestep limitation in the currently used explicit algorithm for the diffusion equation. The assumed value of the resistivity coefficient η is $3 \times 10^{25}\ \mathrm{cm}^2\ \mathrm{s}^{-1}$. The differential rotation is quantified by the shearing parameter $q_{\rm shear} = 1$ corresponding to the flat rotation curve. The values of other input parameters as vertical gravity, gas column density, angular velocity and SN rates for the chosen rings are showed in Table 1. The magnetic field structures obtained from the local calculations at chosen time are replicated into subsequent rings so that the large-scale galactic disk could be constructed.

In order to get the radio emission maps as seen face-on (edge-on) at first we rotate the modeled galaxy at inclination 10° (89°) (see Figure 3 and Otmianowska-Mazur et al. 2008, ApJ, submitted). Then, we integrate the Stokes parameters (I, Q and U) of synchrotron emission along the line of sight, following the standard formulae (see e.g. Longair 1994). The energy distribution of synchrotron-emitting electrons is taken directly from the numerical calculations. Finally, we convolve the calculated maps with a Gaussian beam according to the resolution of the radio continuum observations. The same galaxy model is also prepared according to the real orientation of the NGC 5775 (inclination of 80° and position angle of 145°, Figure 4).

3. RESULTS

3.1. *Growth of magnetic field at different galactocentric radii*

In Figure 2 we show efficiency of the magnetic field amplification observed in our calculations at the subsequent galactocentric distances. First, we note that the fast exponential growth of the total magnetic energy and the azimuthal flux is present for all local models (see Figure 2 top and bottom panels). For instance at the radius 5 kpc we get maximal growth of the total magnetic energy which increase

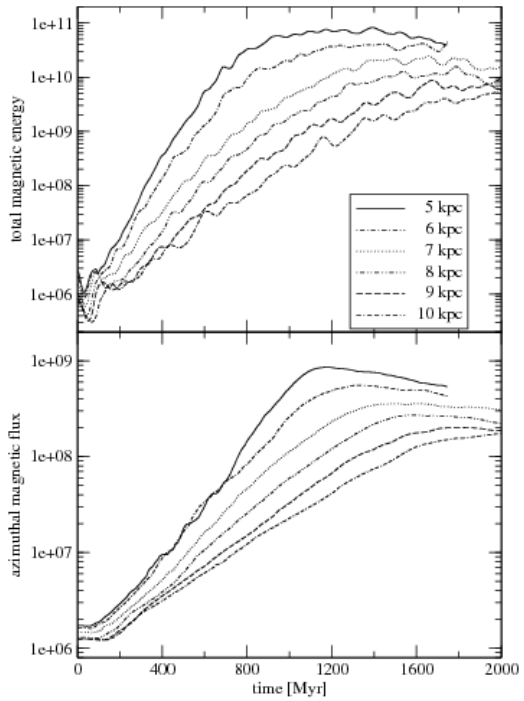

Fig. 2. Growth of magnetic flux and magnetic energy at different R_G.

by 5 orders of magnitude and the magnetic flux by 3 orders of magnitude in time 150 Myr. The magnetic energy and flux grow fast – the faster, the closer is to the galactic center. The discussed radial dependency of the amplification efficiency is connected with the assumed highest SN rate in the region between 4 and 5 kpc. The CR dynamo is more efficient when we apply high SN events. After the amplification phase magnetic energy enters the saturation phase – the earlier, the faster growth rate was observed. The e-folding time determined for the period 200 and 800 Myr are presented in Table 1. At the radius of 5.0 kpc the resulted growth rate is 152 Myr, which is equal to a rotational period of galaxies. Similar e-folding time we get also is for the rest of the radii.

3.2. *Maps of polarized synchrotron emission - different viewing angles*

The polarization maps at two chosen inclinations of the disk: face-on (Figure 3 top panel) and edge-on (Figure 3 bottom panel) at the time-step equal to 0.7 Gyr are presented. The first of them shows polarized emission topolines and vectors constructed by the inclination of 10° (almost face-on). The values of the pitch angles of the polarization vectors range from 10° to 12° (see Table 1). Such topology of the polarized vectors resembles the one observed in reality. The edge-on view (Figure 3 bottom panel) exhibits significant vertical components of the magnetic field seen at intermediate radii of our model. They are seen as detached extensions in all four quadrants of the model galaxy. Most of the emission is polarized in direction parallel to the disk plane, and the narrow depolarized channels are clearly seen between the main galactic body and the extensions. These channels are obviously the effect of so-called beam depolarization, caused by rapid changes of magnetic field directions within the beam size.

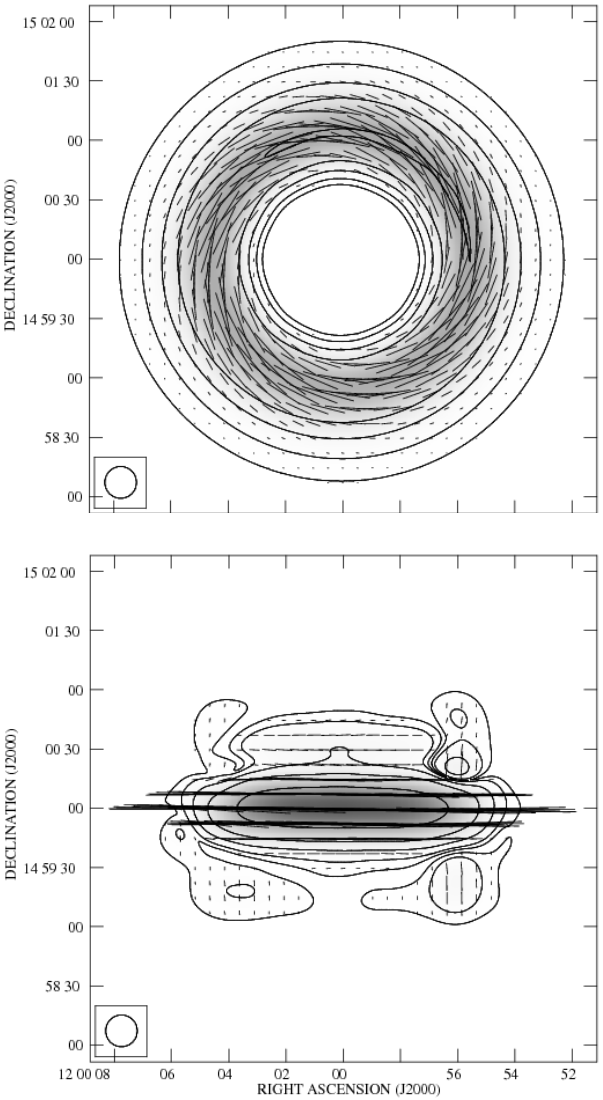

Fig. 3. Face-on (top panel) and edge-on (bottom panel) maps of the polarized emission of the modeled galaxy at the time of 700 Myr. Contours and grey scale show polarized emission intensity, vectors are of directions of apparent magnetic polarization vector, and length proportional to the intensity.

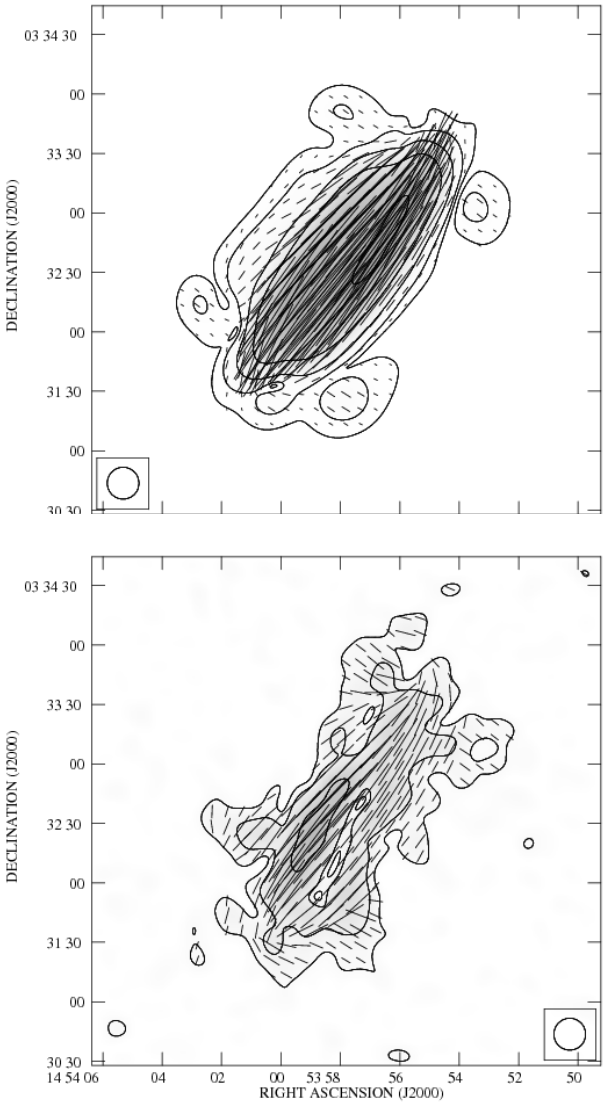

Fig. 4. Map of the modeled galaxy at the latest (2 Gyr) time-step of the evolution (upper pannel) oriented as the real galaxy NGC 5775 (lower panel). Contours and grey scale show polarized emission intensity, vectors are of directions of apparent magnetic polarization vector, and length proportional to the intensity.

3.3. *Comparison: model vs. real galaxy: X-type vertical structures*

In Figure 4 we present the comparison between the polarization emission maps of NGC 5775 (lower pannel) and our model of this galaxy (upper pannel). In both pictures, topolines of polarized intensity are superimposed onto the greyplot of the same quantity, together with vectors of directions of the apparent magnetic polarization with length proportional to the intensity. The polarization vectors in the central part of the modeled galaxy and the real one are similarly parallel to the disk. The extended structures, polarized perpendicularly to the disk plane, are vsible in both maps, as well. However, in the real NGC 5775 the extensions are separated less than in our model. The depolarized channels, clearly seen in the model map is barely visible only in eastern and western extensions in real galaxy. This suggests that in real galaxy the magnetic field changes its orientation more smoothly than in the model.

The only clear differences between the model and the real observations are present close to the major axis of the galaxy. Narrow depolarized channel is seen on the lower pannel of Figure 4. It can be explained by relatively strong Faraday effects close to the disk plane (Soida 2005). Our model does not include the central part ($R < 5$ kpc) of the galaxy, so Faraday effects were not included there.

4. CONCLUSIONS

• CR-driven dynamo amplifies the mean magnetic field on galactic rotation timescale.

• Synthetic radio maps constructed on the base of local shearing box simulations display morphological details (magnetic pitch angles, X-shaped structures) consistent with observed galactic images.

• In Otmianowska-Mazur et al. (2007) we also show that our modeled EMF is fully nonlinear and it is not possible to apply any of the considered nonlinear dynamo approximations due to the fact that the conditions for the scale separation are not fullfiled.

Necessary improvements:

• Enlargement of CR diffusion coefficients $K_{\parallel}$, $K_{\perp}$ to realistic values, by an order of magnitude.

• Global galactic disk simulations → escape of CR along horizontal magnetic filed in galactic plane, to avoid the CR excess.

This work was partly supported by a grant from the Polish Ministry of Science, grant no. PB 2693/H03/2006/31

REFERENCES

Berezinskii, V. S., Bulanov, S. V., Dogiel, V. A., Ginzburg, V. L., & Ptuskin, V. S. 1990, Astrophysics of Cosmic Rays (Amsterdam: North-Holland)
Brandenburg, A., & Dobler, W. 2001, A&A, 369, 329
Brandenburg, A., & Sokoloff, D. D. 2002, Geophys. Astrophys. Fluid Dynamics, 96, 319
Dumke, M., Krause, M., Wielebinski, R., & Klein, U. 1995, A&A, 302, 691
Giacalone, J., & Jokipii, R. J. 1999, ApJ, 520, 204
Ellison, D. C., Decoruchelle, A., & Ballet, J. 2004, A&A, 413, 189
Hanasz, M., & Lesch, H. 2003, A&A, 412, 331

Hanasz, M., Kowal, G., Otmianowska-Mazur, K., & Lesch, H. 2004, ApJ, 605, L33
Hanasz, M., Otmianowska-Mazur, K., Kowal, G., & Lesch, H. 2006, Astron. Narcht., 327, 469
Heesen, V., Krause, M., Beck, R., & Dettmar, R.-J. 2005, Proc. of the MPGE 2004, Jagiellonian University Press), 156
Jokipii, J. R. 1999, in Interstellar Turbulence, ed. J. Franco & A. Carraminana (Cambridge: Cambridge Univ. Press), 70
Kowal, G., Hanasz, M., & Otmianowska-Mazur, K. 2003, A&A, 404, 533
Kuwabara, T., Nakamura, K., & Ko, C. M. 2004, ApJ, 607, 828
Longair, M. S. 1994, High Energy Astrophysics (Cambridge: Cambridge Univ. Press)
Mac Low, M., & Klessen, 2004, Rev. Mod. Phys., 76, 125
Otmianowska-Mazur, K., Kowal, G., & Hanasz, M. 2007, ApJ, 668, 110
Parker, E. N. 1992, ApJ, 401, 137
Ryu, D., Kim, J., Hong, S. S., & Jones, T. W. 2003, ApJ, 589, 338
Schlickeiser, R., & Lerche, I. 1985, A&A, 151, 151
Snodin, A. P., Brandenburg, A., Mee, A. J., & Shukurov, A. 2006, MNRAS, 373, 643
Soida, M. 2005, The Magnetized Plasma in Galaxy Evolution, ed. K. Chyzy, K. Otmianowska-Mazur, M. Soida, & R.-J. Dettmar (Fraków: Jagiellonian Univ. Press), 185
Tüllmann, R., Dettmar, R.-J., Soida, M., Urbanik, M., & Rossa, J. 2000, A&A, 364, L36
Widrow, L. M. 2002, Rev. Mod. Phys., 74, 775